Soft conductive micropillar electrode arrays for biologically relevant electrophysiological recording

Yuxin Liu[a,1], Allister F. McGuire[b,1], Hsin-Ya Lou[b], Thomas L. Li[b], Jeffrey B.-H. Tok[c], Bianxiao Cui[b,2], and Zhenan Bao[c,2]

[a]Department of Bioengineering, Stanford University, Stanford, CA 94305; [b]Department of Chemistry, Stanford University, Stanford, CA 94305; and [c]Department of Chemical Engineering, Stanford University, Stanford, CA 94305

Edited by Peidong Yang, University of California, Berkeley, Lawrence Berkeley National Laboratory, Berkeley, CA, and approved September 26, 2018 (received for review June 25, 2018)

Multielectrode arrays (MEAs) are essential tools in neural and cardiac research as they provide a means for noninvasive, multiplexed recording of extracellular field potentials with high temporal resolution. To date, the mechanical properties of the electrode material, e.g., its Young's modulus, have not been taken into consideration in most MEA designs leaving hard materials as the default choice due to their established fabrication processes. However, the cell–electrode interface is known to significantly affect some aspects of the cell's behavior. In this paper, we describe the fabrication of a soft 3D micropillar electrode array. Using this array, we proceed to successfully record action potentials from monolayer cell cultures. Specifically, our conductive hydrogel micropillar electrode showed improved signal amplitude and signal-to-noise ratio, compared with conventional hard iridium oxide micropillar electrodes of the same diameter. Taken together, our fabricated soft micropillar electrode array will provide a tissue-like Young's modulus and thus a relevant mechanical microenvironment to fundamental cardiac and neural studies.

soft conductive hydrogel microelectrode | electrophysiological recording | micropillar electrode

High-quality and reliable electrophysiological recording is critical in the study of both the nervous and cardiac systems and has thus been widely pursued (1–7). To achieve accurate electrophysiological measurements, high sealing resistance to prevent leakage current and low impedance across the cell–electrode interface are required (8–10). Recent studies have demonstrated that 3D electrodes, e.g., vertical micropillars and nanopillars, are able to achieve intracellular recording (9, 11, 12). In addition, these multielectrode arrays (MEAs) with 3D electrodes have shown improved signal amplitude and quality compared with traditional planar-electrode MEAs. Specifically, the electrodes' 3D geometry was able to decrease the electrode impedance at a given electrode diameter by increasing the electrode surface area and to induce the cells to engulf the electrodes, thus forming an excellent seal with the cell membrane in vitro (11, 13).

For the fabrication of 3D electrodes, it is common to use traditional conductors, such as iridium oxide, gold, or platinum, to interface with electrogenic cells (9, 13). However, the Young's moduli of these materials (greater than hundreds of GPa) are several orders of magnitude higher than that of the electrogenic cells and tissues (1–100 kPa) (14), leading to a significant mechanical mismatch at the cell–electrode interface. Recent studies have revealed that local mechanical cues, such as the Young's modulus (15, 16) and apparent stiffness (17) of the interfacing materials, can translate to biochemical signals. These biochemical signals subsequently control multiple aspects of cell behavior, such as growth and differentiation. In addition, mechanical memory from past physical environments can be stored by intracellular transcriptional activators such as YAP/TAZ [Yes-associated protein (YAP) and its transcriptional coactivator with PDZ-binding motif (TAZ)] that act as an intracellular mechanical rheostat, which ultimately influences the cells' behavior (18). Therefore, in addition to the electrochemical properties of electrode materials, the mechanical properties of the electrodes must also be taken into consideration when designing the electrode–cell interface.

Results and Discussion

We hypothesized that conductive hydrogels represent ideal candidate materials for mechanically matched electrodes due to their tissue-like softness. However, the low conductivity of most hydrogels has previously limited their application in functional electrophysiological recording. Recently, we developed a type of hydrogel that is highly conductive, water-stable, biocompatible, with a tissue-level Young's modulus: electrically conductive hydrogel (ECH). In this work, we use the material to fabricate 3D, hydrogel-based soft micropillar electrode arrays (ECH-MEAs) for electrophysiological recording in vitro. We observed that our fabricated soft micropillars yielded to cardiomyocytes' contraction–relaxation cycles, thus minimizing any impediment to the natural, rhythmic beating of the cells (Fig. 1*A*). For the fabrication of the ECH-MEAs, poly(3,4-ethylenedioxythiophene) polystyrene sulfonate (PEDOT:PSS) ECH modified with a highly conductive ionic liquid was used as the electrode material. An array of 60 ECH micropillars with an average diameter of 3 μm was lithographically patterned on top of platinum interconnects on a transparent glass substrate. Each micropillar is independently addressable and connected to a multichannel electrophysiological system via a printed circuit board.

Significance

The large mechanical discrepancy at the cell–electrode interface (~6 orders of magnitude difference in Young's moduli) is known to significantly affect the cell's behavior and its mechanotransduction pathways. To date, the Young's moduli of the electrode materials do not match those of the cells, due to the limited availability of required electronic materials for microfabrication. Here, we present a soft micropillar electrode array made of electronically conductive hydrogel as a general tool for electrophysiological recording. The three-dimensional microelectrode provides biologically relevant mechanical microenvironment to the cells during electrophysiological recording with higher amplitude and signal-to-noise ratio compared with a state-of-the-art inorganic microelectrode.

Author contributions: Y.L., A.F.M., H.-Y.L., B.C., and Z.B. designed research; Y.L., A.F.M., and T.L.L. performed research; Y.L., A.F.M., B.C., and Z.B. analyzed data; and Y.L., A.F.M., J.B.-H.T., B.C., and Z.B. wrote the paper.

The authors declare no conflict of interest.

This article is a PNAS Direct Submission.

[1]Y.L. and A.F.M. contributed equally to this work.

[2]To whom correspondence may be addressed. Email: bcui@stanford.edu or zbao@stanford.edu.

This article contains supporting information online at www.pnas.org/lookup/suppl/doi:10.1073/pnas.1810827115/-/DCSupplemental.

Published online October 30, 2018.

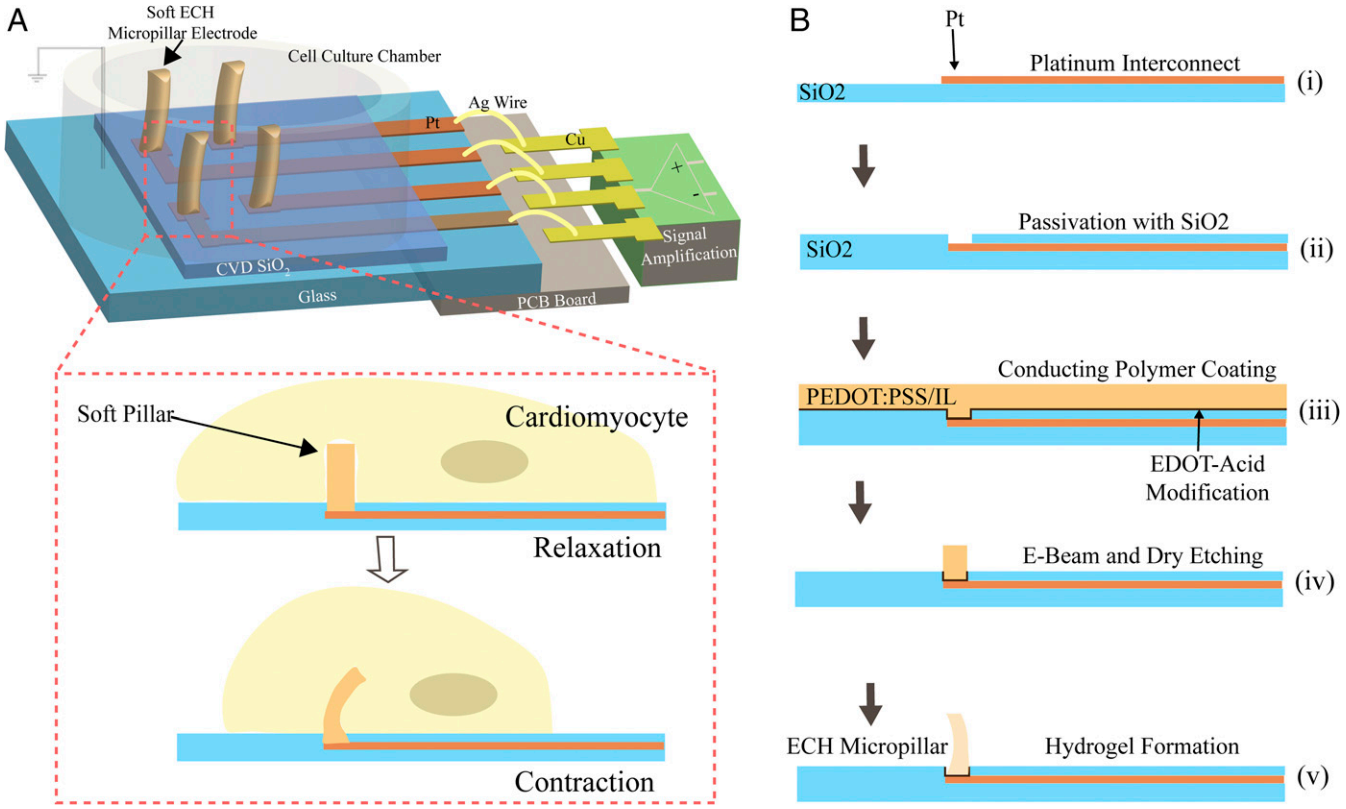

Fig. 1. Schematic illustration of a soft conductive hydrogel micropillar array for electrophysiological recording and its fabrication process. (*A*) Soft MEA with ECH micropillar electrode for electrophysiological recording of cardiomyocytes. The platinum interconnects were passivated by chemical-vapor-deposited (CVD) silicon oxide and wire-bonded to a printed circuit board (PCB). Hydrogel micropillars bend with engulfing cardiomyocytes, reducing perturbations to the beating of the cardiomyocytes. (*B*) Fabrication process: Platinum was photolithographically patterned on a glass wafer (feedlines 3 μm wide, 50 nm thick) (*B*, *i*), followed by deposition and patterning of silicon dioxide as a passivation layer (0.8 μm thick) (*B*, *ii*). An aqueous solution of PEDOT:PSS and IL was then drop casted (1.8 μm) (*B*, *iii*) and patterned by electron beam lithography and reactive-ion etching (*B*, *iv*) to give diameter of 3 μm. Finally, the conductive hydrogel micropillar was formed by soaking in water for 4 h (*B*, *v*).

Micropatterning hydrogel materials to produce a high aspect ratio remains a challenge due to their high water content. Here, we describe a simple process for fabricating the 3D ECH-MEA (Fig. 1*B*; see *SI Appendix* for details). First, platinum interconnects were micropatterned on a glass substrate using conventional photolithography and passivated by chemical-vapor-deposited silicon dioxide (0.8 μm thick). In the passivation layer, we etched 3-μm-diameter holes at the termini of the platinum interconnects. Second, we modified the platinum surface with 2,3-dihydrothieno (3,4-b)(1,4)dioxine-2-carboxylic acid (EDOT-acid) to improve hydrogel–platinum adhesion according to a previously reported method (20). An aqueous mixture of PEDOT:PSS and ionic liquid, 4-(3-Butyl-1-imidazolio)-1-butanesulfonic acid triflate, was then drop cast and baked at 130 °C. Mixing the ionic liquid into PEDOT:PSS improves the conductivity via morphological modification. In addition, the ion gel serves as the precursor to hydrogel and allows for conventional microfabrication. The dried ion gel was micropatterned with electron beam lithography and dry etched with Au as a hard mask. Last, the water-soluble ionic liquid was removed by soaking in aqueous solution to afford the hydrogel micropillar. To compare the electrochemical properties between our fabricated ECH micropillar electrode and a planar electrode, we measured the impedance of the device before and after depositing the ECH micropillars. We observed that the electrodes with ECH micropillars showed more than one order of magnitude lower impedance (measured at 1 kHz) compared with that of the platinum planar electrodes (*SI Appendix*, Fig. S1).

The ECH-MEA was wire-bonded onto a printed circuit board and a plastic chamber was glued on the chip to contain cell culture media. Scanning electron microscopy (SEM) indicated that the dry micropillar has a height of 1.8 μm, with an aspect ratio of 0.59 (Fig. 2*A*). Upon rehydration in phosphate-buffered saline (PBS) solution, the anisotropic swelling properties of the micropillar resulted in a significant increase in its aspect ratio to 4.3. The swelling appeared to occur anisotropically in the out-of-plane direction (*SI Appendix*, Fig. S2) since the diameter at the rehydrated pillar remained almost unchanged at 3 μm. To demonstrate that the ECH micropillar electrode is soft and flexible, we generated fluid flow by injecting 10 μL of PBS to the micropillar area already immersed in PBS. Under the flow, we observed that each of the ECH micropillars was able to bend around its central axis (Fig. 2 *B* and *C*), whereas a stiff iridium oxide electrode with the same diameter was unable to bend under the same conditions (*SI Appendix*, Fig. S3 and Movie S1). Furthermore, when cell line HL-1 mouse cardiac muscle cells (21) were cultured on the ECH micropillar array, the beating of the muscle cells was sufficient to displace the pillars at the cell beating frequency. (Movie S2). These results confirm that the hydrogel microelectrodes are soft and bendable in physiological conditions. The bending of the micropillar minimally affects electrophysiological recording of action potentials when recording from cardiomyocytes during contraction–relaxation cycles due to the insensitivity of the electrochemical impedance to bending (<3% change) of the ECH material (*SI Appendix*, Fig. S4).

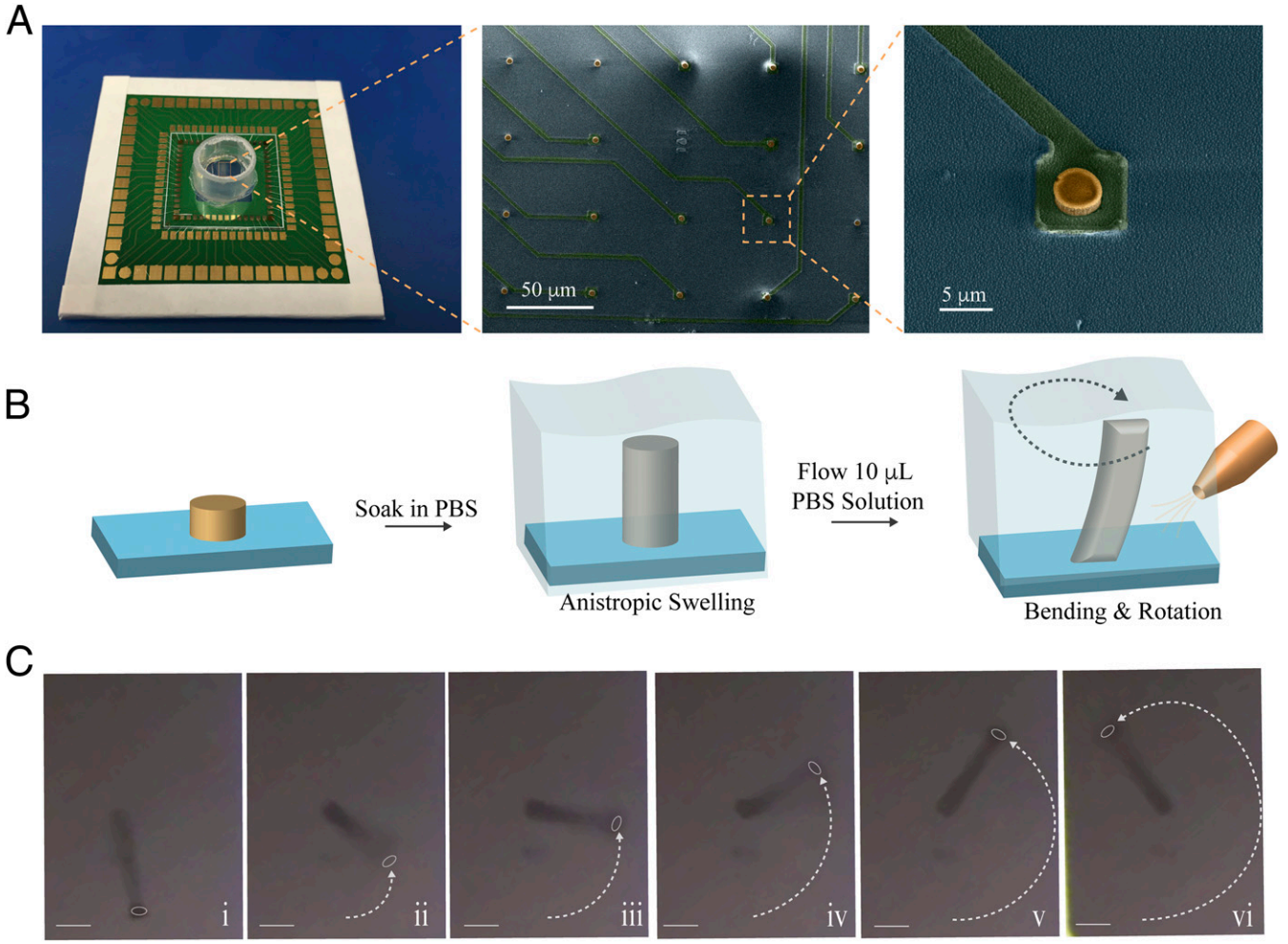

Fig. 2. Soft and flexible ECH micropillars (*A*, *Left*) Soft MEA with an array of ECH micropillar electrodes. (*A*, *Middle*) False-colored SEM image of an array of dehydrated ECH micropillar electrodes. (Scale bar: 50 μm.) (*A*, *Right*) Zoomed-in SEM image of dehydrated ECH micropillar patterned on top of a platinum interconnect (height 1.8 μm; diameter 3 μm). (Scale bar: 5 μm.) Yellow: dehydrated ECH micropillar. Green: platinum interconnect passivated by SiO_2. Light blue: SiO_2 substrate. (*B*) Schematic illustration of formation of an ECH micropillar by soaking in PBS. The ECH swells anisotropically in out of plane direction and the ECH micropillar bends and rotates during infusing PBS solution (10 μL). (*C*) Optical microscope image of ECH micropillar bending and rotating when 10 μL of PBS solution is infused. (Scale bars: 5 μm.)

Next, the ECH-MEA was used to record action potentials from HL-1 cells. After culturing the cells in the chamber for 2 d, increased electrode impedance suggested the formation of a tight interface between the cell membrane and electrode (*SI Appendix*, Fig. S5). We were able to record extracellular HL-1 cell action potentials from both an ECH micropillar and an iridium oxide micropillar (both 3 μm in diameter). Our data show that ECH micropillar electrodes record signals with larger amplitude than iridium oxide electrodes (i.e., 156.1 μV vs. 80.5 μV, Fig. 3 *A*–*C*). In addition, the ECH micropillar has ∼10-fold improvement in its signal-to-noise ratio (S/N = 33.7) compared with that of the iridium oxide micropillar (S/N = 3.1, Fig. 3*D*). We attributed this significantly improved signal strength and signal-to-noise ratio to an overall reduction in electrode impedance (Fig. 3*E*). This is enabled by the high volumetric capacitance and excellent ionic and electrical dual conductivity of the ECH, stemming from its highly porous nanostructure (19). Furthermore, the soft ECH micropillar electrode was able to electrically stimulate HL-1 cells with the intent to pace them. HL-1 cells were paced with short pulses with a frequency of 1 Hz and an amplitude of 1 V through the ECH microelectrode. Extracellular potentials were subsequently recorded by the same electrodes which showed a pace frequency of 1 Hz (*SI Appendix*, Fig. S6).

We next focused on characterizing the mechanical interface between cells and the electrodes. It is well known that there is a significant mechanical mismatch between cells (14) and previous 3D microelectrodes, such as Au mushroom-shaped microelectrodes (12), SiO_2/Pt nanoelectrodes (6), iridium oxide microelectrodes, and Pt nanoelectrodes (11). We hypothesize that our fabricated ECH pillar electrode will greatly reduce the mechanical mismatch between cells and electrodes without the need for any additional coatings or modifications, while maintaining good performance in electrophysiological recording. Indeed, our ECH micropillar represents a 3D microelectrode with a tissue-like Young's modulus measured at 13.4 kPa. (Fig. 4*A* and *SI Appendix*, Fig. S7).

Cells' local topographical and mechanical environments play a critical role in regulating their mechanotransduction pathways. For example, YAP and TAZ are the sensors and mediators of mechanical cues provided by the cellular microenvironment, such as the Young's modulus (15). Specifically, stiff microenvironmental cues will trigger YAP/TAZ nuclear localization and activate the Hippo signaling pathway, which has been implicated

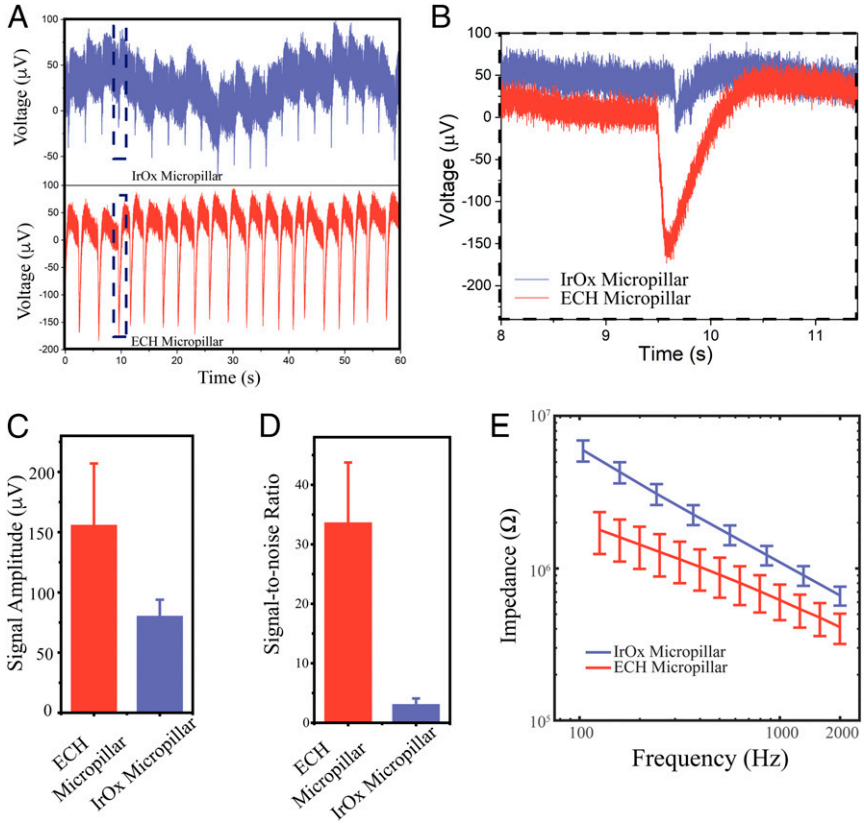

Fig. 3. Electrophysiological recording with the ECH micropillar. (*A*) Extracellular recording of cardiomyocytes with conventional IrOx micropillar (*Top*) and soft ECH micropillar (*Bottom*) electrode with the same diameter of 3 μm. (*B*) Zoomed-in extracellular recording from the black box in *A*. (*C*) Signal amplitude and (*D*) signal-to-noise ratio of soft ECH versus IrOx micropillars. Error bars denote SD (IrOx $n = 6$; ECH $n = 6$). (*E*) Potentiostatic electrochemical impedance spectroscopy of ECH micropillars compared with IrOx micropillars with the same diameter at electrophysiologically relevant frequencies. Error bars denote SEM ($n = 49$ IrOx, $n = 50$ ECH).

in cell migration, cell fate determination, and subsequent proliferation (22–25). To investigate the cellular response to our ECH material as a potential environmental cue, we proceeded to seed HL-1 cells on both glass and ECH substrates. Here, the stiff glass substrate acts as a control because it has a similar Young's modulus to conventional electrode materials, such as Au and iridium oxide. Immunochemical staining was then applied to evaluate the spatial distribution of YAP/TAZ for the cells cultured on both glass (Young's modulus of approximately tens of GPa) and ECH substrates (Young's modulus of approximately tens of kPa). Our results indicated that YAP/TAZ is almost evenly distributed between the cells' cytoplasm and nucleus when cultured on the ECH substrate, whereas YAP/TAZ is concentrated in the cell nucleus when seeded on the glass substrate (Fig. 4 *B* and *C*). Subsequent statistical analysis of fluorescence intensity ratio between the cell's nucleus and cytoplasm revealed that cytoplasmic localization of YAP/TAZ is significantly higher on ECH, compared with using glass as the growth substrate. (Fig. 4*D*) These results suggest that the local mechanical microenvironment of ECH resembles, and is thus highly compatible with, the softness of tissue in vivo.

Conclusions

In summary, this work has illustrated that soft electrically and ionically conductive ECH micropillar electrodes are promising 3D electrodes for biologically relevant electrophysiology measurements. Specifically, we have successfully developed a simple fabrication process to enable electrically conductive hydrogel-based soft micropillar electrodes possessing high aspect ratios. This was accomplished by using the unique anisotropic swelling properties of PEDOT:PSS-based ECH. Our fabricated ECH micropillar electrode was observed to possess both a higher signal-to-noise ratio and stronger signal strength compared with a conventionally employed iridium oxide micropillar of the same diameter. More importantly, our ECH micropillar significantly reduces the mechanical mismatch at the electrode-cell interface, and this achievement represents a 3D microelectrode with tissue-like mechanical properties.

Materials and Methods

Material Preparation. PEDOT:PSS ECH was prepared according to our previously reported method with modification. (19) PEDOT:PSS (PH1000) and the ionic liquid [IL, 4-(3-Butyl-1-imidazolio)-1-butanesulfonic acid triflate] were purchased from Clevios and Santa Cruz Biotechnology, respectively. About 50 wt % of IL vs. PEDOT:PSS was added to PEDOT:PSS aqueous solution (0.172 g in 15 mL of PH1000 solution) and stirred vigorously for 20 min. The PEDOT:PSS/IL aqueous mixture was then filtered by a 0.45-μm syringe filter before drop casting.

Device Fabrication.

General microelectrode array fabrication. First, Ti (5 nm) and Pt (50 nm) were evaporated via electron beam (Innotec) on a clean 4-in. Pyrex glass wafer. Interconnects were micropatterned using conventional photolithography. The positive photoresist (Shipley 3612) was exposed with a contact mask aligner (Karlsuss). Dry etching via Ar bombardment (Materials Research Corp.) was used to etch the exposed Ti and Pt. Subsequently, 0.8 μm of SiO_2 was deposited via plasma-enhanced chemical vapor deposition (350 °C; Plasma-Therm Shuttlelock). To create 3-μm-diameter microholes in the passivation, a thick photoresist layer (4-μm Shipley 220–3) was patterned with contact photolithography at the termini of the platinum interconnects. Dry etching via Plasma-Therm Versaline oxide etcher (45 sccm CHF_3, 5 standard cubic centimeters per minute O_2, bias 50 V) created vias to the Pt surface. The glass wafer was diced into 2 cm × 2 cm pieces by a wafer saw (DISCO Wafer Saw

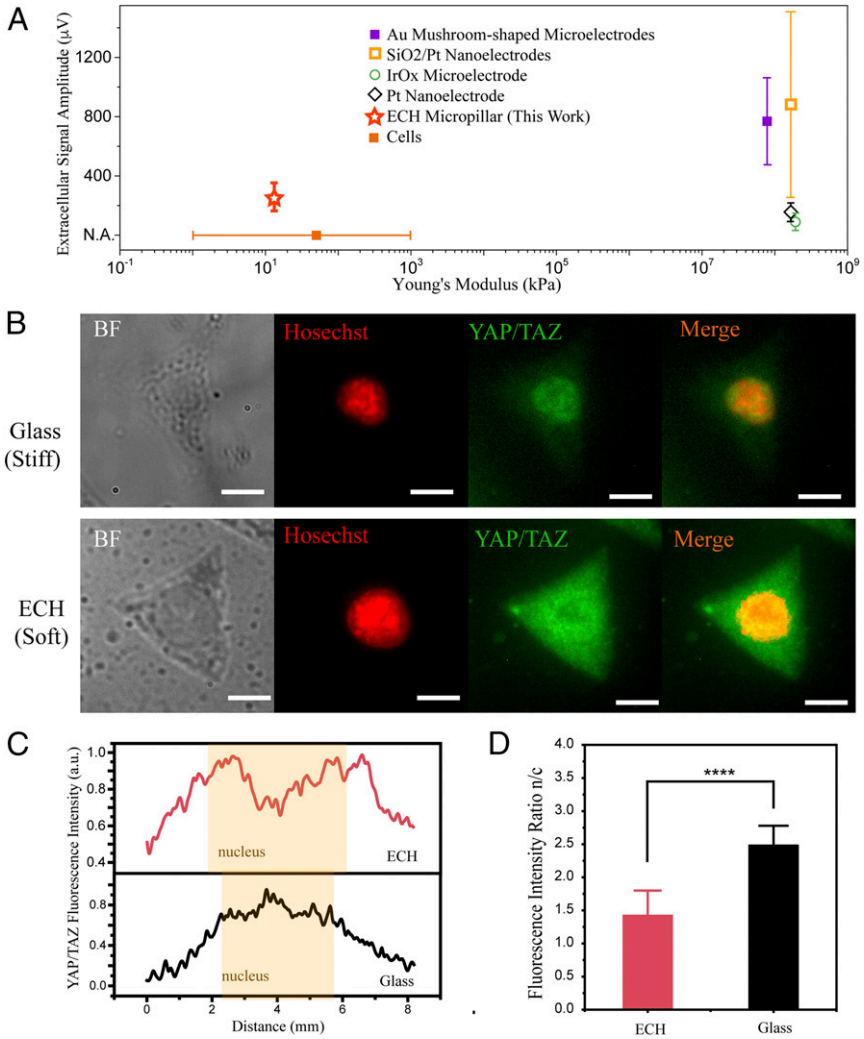

Fig. 4. ECH mimics the mechanical microenvironment of soft tissue (*A*) Extracellular recording amplitude and Young's modulus of the MEA in this work compared with those of representative 3D electrode arrays. The Young's modulus of the ECH micropillar is within the range of Young's modulus of cells (14) and significantly lower compared with Au mushroom-shaped microelectrode (12), SiO_2/Pt nanoelectrode (6), IrOx microelectrode, and Pt nanoelectrode (11). (*B*) Immunofluorescence images of endogenous YAP/TAZ subcellular localization on glass and ECH substrates. (Scale bars: 5 μm.) (*C*) Fluorescence intensity as a function of distance across the cell for ECH and glass substrates. YAP/TAZ has greater localization to the cytoplasm for cells on an ECH substrate compared with those on a glass substrate. (*D*) Statistical analysis of immunofluorescence intensity ratio of YAP/TAZ between nucleus and cytoplasm ($n = 12$; ****$P < 0.0001$; Student's t test).

DAD3240), yielding multielectrode arrays patterned with ∼3.5-μm-deep holes in photoresist.

PEDOT pillar fabrication. For each piece, the photoresist mask was stripped in acetone. Thereafter, the platinum surface was modified with EDOT-acid to improve hydrogel-platinum adhesion according to a previously reported method (20). Briefly, the ozone-treated (30 min, UVO-cleaner model no. 42, Jetlight) device was immersed into a 10-mM ethanol solution of EDOT-acid at room temperature overnight to ensure the formation of a densely packed monolayer. The substrate was then rinsed with acetonitrile to remove any residual EDOT-acid. The prepared aqueous mixture of PEDOT:PSS and IL (the estimated weight ratio between PEDOT:PSS and IL is ∼1) was then drop cast and dried overnight (∼2 μm), followed by a 20-min hotplate bake at 130 °C. A 40-nm Au hard mask was deposited by KJ Lesker electron beam evaporator. Raith 150 electron beam writer was used to pattern the Ma-N 2403 resist (MicroChem) on the Au hard mask. Ion milling (500 W; Intlvac Nanoquest Ion Mill) was used to etch away the exposed Au. Plasma-Therm Versaline oxide etcher (40 sccm O_2, bias 50 V) was used to etch the dried PEDOT:PSS/IL ion gel. Subsequently, the water-soluble IL was removed by soaking in water for 4 h and the substrate air dried. The chip was wire bonded to a PCB and a plastic chamber was glued (RTV 108) to the glass to contain culture media.

Iridium oxide pillar fabrication. Taking the insulated multielectrode array still coated in thick resist, iridium oxide (IrOx) was electrodeposited from a colloidal solution (to a thickness of 2.5 μm). The solution was prepared according to a previously reported method (13). Potentiostatic deposition proceeded at 0.55 V vs. Ag/AgCl/sat. KCl. Subsequently, the photoresist support was stripped in acetone, the chip wirebonded to a PCB, and a plastic chamber attached.

Device Characterization. Impedance and cyclic voltammetry of the ECH and IrOx micropillars were measured with potentiostat Bio-Logic SP-200. PBS or culture media Claycomb medium was used as the electrolyte and Ag/AgCl/sat. KCl was used as the reference electrode. Bending and rotation of the ECH micropillar was induced by infusing of 10 μL PBS solution with micropipette. The Young's modulus of the ECH bulk material (6 mm × 6 mm with thickness of 0.05 mm) was characterized by measurement of the stress–strain curve with a pressure station (Newmark Systems and BG Series Digital Force Gauge). The Young's modulus was calculated as the ratio of compressive stress to the strain from the linear region (<10% strain). The bending test was carried out in PBS solution. The electrochemical impedance of the ECH pillar (cross-sectional area: 1 mm^2; height: 4.3 mm) was measured before and after bending with curvatures of 0.077, 0.14, and 0.4 mm^{-1}.

Cell Culture and Immunostaining. The HL-1 cardiomyocyte cell line was obtained from the laboratory of William C. Claycomb at Louisiana State

University. To facilitate cell attachment, the culture chamber was coated with 5 μg/mL fibronectin in 0.02% gelatin solution for 1 h. HL-1 cells were then seeded inside the chamber at a density of $\sim 1 \times 10^5$ cm^{-2}. A standard incubator at 37 °C and 5% CO_2 was used. Claycomb medium supplemented with 10% fetal bovine serum, 0.1 mM norepinephrine, 2 mM L-glutamine, 100 U/mL penicillin, and 100 μg/mL streptomycin was changed every 24 h.

For immunofluorescence studies, cells were fixed with freshly prepared 4% (0.04 g/mL) paraformaldehyde for 10–15 min and then rinsed with PBS three times. To permeabilize the cells, cells were incubated in 0.1% Triton-X 100 in PBS for 15 min followed by rinsing with PBS three times. Then, the cells were incubated in blocking solution (3% BSA in PBS + 0.1% Tween) for 1 h at room temperature with mild agitation. The cells were then incubated in blocking solution containing primary antibodies, YAP Antibody (dilution 1:200, sc-101199; Santa Cruz Biotechnology) for 1 h at room temperature, followed by a rinse with PBS + 0.1% Tween three times (5 min each). Subsequently, the cells were incubated with secondary antibodies in blocking solution for 30–45 min at room temperature. The nucleus was stained with Hoescht 33258 (dilution 1:5,000) at room temperature for 30 min. Lastly, the cells were rinsed with blocking buffer twice (5 min each).

Fluorescence and bright-field images were taken using an inverted microscope (Leica DMI6000 B). ImageJ and CellProfiler were used to analyze the fluorescence intensity. Student's *t* test was used for the immunostaining study ($n = 12$; *P < 0.05; ****P < 0.0001).

Electrophysiological Recording in Vitro. A 60-channel voltage amplifier system (MEA1060-Inv-BC; Multichannel System) was used to record HL-1 cells cultured on the micropillar arrays after the cells started beating. Recording was performed with a Ag/AgCl electrode in the medium as the reference electrode and the sampling rate was 5–20 kHz. The signal was filtered with a band-pass of 1 Hz–5 kHz. For electrical pacing, biphasic pulses with pulse width of 200 μs and amplitude of 1 V were applied to the micropillar electrode at 1 Hz. The same electrode was used to record extracellular action potentials followed by pacing.

ACKNOWLEDGMENTS. This work was partly supported by a Bio-X Interdisciplinary Initiatives Seed Grant and by the National Institutes of Health under Award R01-GM125737. Part of this work was performed at the Stanford Nano Shared Facilities (SNSF), supported by the National Science Foundation under Award ECCS-1542152. Y.L. is supported by a National Science Scholarship (A*STAR, Singapore). A.F.M. is supported by a Stanford Bio-X Graduate Fellowship.

1. Khodagholy D, et al. (2015) NeuroGrid: Recording action potentials from the surface of the brain. *Nat Neurosci* 18:310–315.
2. Khodagholy D, et al. (2013) In vivo recordings of brain activity using organic transistors. *Nat Commun* 4:1575.
3. Qi D, et al. (2017) Highly stretchable, compliant, polymeric microelectrode arrays for in vivo electrophysiological interfacing. *Adv Mater* 29:1702800.
4. Minev IR, et al. (2015) Biomaterials. Electronic dura mater for long-term multimodal neural interfaces. *Science* 347:159–163.
5. Duan X, et al. (2011) Intracellular recordings of action potentials by an extracellular nanoscale field-effect transistor. *Nat Nanotechnol* 7:174–179.
6. Abbott J, et al. (2017) CMOS nanoelectrode array for all-electrical intracellular electrophysiological imaging. *Nat Nanotechnol* 12:460–466.
7. Liu J, et al. (2015) Syringe-injectable electronics. *Nat Nanotechnol* 10:629–636.
8. Fromherz P, Offenhäusser A, Vetter T, Weis J (1991) A neuron-silicon junction: A Retzius cell of the leech on an insulated-gate field-effect transistor. *Science* 252:1290–1293.
9. Robinson JT, et al. (2012) Vertical nanowire electrode arrays as a scalable platform for intracellular interfacing to neuronal circuits. *Nat Nanotechnol* 7:180–184.
10. Spira ME, Hai A (2013) Multi-electrode array technologies for neuroscience and cardiology. *Nat Nanotechnol* 8:83–94.
11. Xie C, Lin Z, Hanson L, Cui Y, Cui B (2012) Intracellular recording of action potentials by nanopillar electroporation. *Nat Nanotechnol* 7:185–190.
12. Hai A, et al. (2009) Spine-shaped gold protrusions improve the adherence and electrical coupling of neurons with the surface of micro-electronic devices. *J R Soc Interface* 6:1153–1165.
13. Lin ZC, Xie C, Osakada Y, Cui Y, Cui B (2014) Iridium oxide nanotube electrodes for sensitive and prolonged intracellular measurement of action potentials. *Nat Commun* 5:3206.
14. Akhtar R, Sherratt MJ, Cruickshank JK, Derby B (2011) Characterizing the elastic properties of tissues. *Mater Today (Kidlington)* 14:96–105.
15. Dupont S, et al. (2011) Role of YAP/TAZ in mechanotransduction. *Nature* 474:179–183.
16. Wen JH, et al. (2014) Interplay of matrix stiffness and protein tethering in stem cell differentiation. *Nat Mater* 13:979–987.
17. Cai P, et al. (2016) Bio-inspired mechanotactic hybrids for orchestrating traction-mediated epithelial migration. *Adv Mater* 28:3102–3110.
18. Low BC, et al. (2014) YAP/TAZ as mechanosensors and mechanotransducers in regulating organ size and tumor growth. *FEBS Lett* 588:2663–2670.
19. Wang Y, et al. (2017) A highly stretchable, transparent, and conductive polymer. *Sci Adv* 3:e1602076.
20. Wei B, Liu J, Ouyang L, Kuo CC, Martin DC (2015) Significant enhancement of PEDOT thin film adhesion to inorganic solid substrates with EDOT-acid. *ACS Appl Mater Interfaces* 7:15388–15394.
21. Claycomb WC, et al. (1998) HL-1 cells: A cardiac muscle cell line that contracts and retains phenotypic characteristics of the adult cardiomyocyte. *Proc Natl Acad Sci USA* 95:2979–2984.
22. Hindley CJ, et al. (2016) The Hippo pathway member YAP enhances human neural crest cell fate and migration. *Sci Rep* 6:23208.
23. Nukuda A, et al. (2015) Stiff substrates increase YAP-signaling-mediated matrix metalloproteinase-7 expression. *Oncogenesis* 4:e165.
24. Ma X, et al. (2017) Hippo signaling promotes JNK-dependent cell migration. *Proc Natl Acad Sci USA* 114:1934–1939.
25. Panciera T, Azzolin L, Cordenonsi M, Piccolo S (2017) Mechanobiology of YAP and TAZ in physiology and disease. *Nat Rev Mol Cell Biol* 18:758–770.